



# Bond behaviour of prestressed basalt textile reinforced concrete

Mohammed Hutaibat<sup>a,b</sup>, Bahman Ghiassi<sup>c,\*</sup>, Walid Tizani<sup>a</sup>

<sup>a</sup> Centre for Structural Engineering and Informatics, Faculty of Engineering, University of Nottingham, Nottingham NG7 2RD, United Kingdom

<sup>b</sup> Department of Civil Engineering, Middle East University, Amman 11831, Jordan

<sup>c</sup> School of Engineering, University of Birmingham, Birmingham B15 2TT, United Kingdom

## ARTICLE INFO

### Keywords:

Textile Reinforced Concrete  
TRC  
Prestressing  
Prestressed TRC  
Pull-out test  
Basalt reinforcement, Bond behaviour

## ABSTRACT

Innovative Textile Reinforced Concrete (TRC) composites, although holding a significant potential, usually have poor performance under serviceability conditions. Addressing this limitation requires applying innovative techniques, such as prestressing, to utilise its potential fully. However, successful design and application of prestressing require a comprehensive understanding of the prestressing effect across scales, including the textile-to-matrix bond behaviour. To address this need, this study investigated the influence of key parameters such as prestressing level, prestressing release time and matrix age on the bond behaviour of basalt textile reinforcement. Test results show a significant influence of prestressing level and release time on textile-matrix bond behaviour. A 1-day prestressing release time resulted in a 25 % increased stiffness with only a 5 % peak load reduction followed by a further 13.7 % increase in the pull-out energy when the prestressing level was 13 %. At 35 % prestress level, 1-day released samples showed a significant reduction of 48.4 % in the peak load and 76 % reduction in the debonding energy. The positive effect of prestressing on the bond behaviour became more evident at prolonged release durations. The 7-day release samples showed a 17.4 % increase in the peak load at both prestress levels. Meanwhile, at 35 % prestress level, 34 % further increase in the debonding energy was observed. The obtained data are then utilised for providing indications on the effect of prestressing on saturated crack spacing of TRC components.

## 1. Introduction

Textile reinforced concrete (TRC) has emerged as an advanced construction material, garnering significant attention for its versatility in retrofitting existing structures or manufacturing new structural components. Its distinctive combination of non-corrosive properties, high tensile strength, flexibility and quasi-ductile behaviour enables the production of slender yet resilient structural elements [1–3]. The textile reinforcement, composed of continuous filaments primarily made of carbon, aramid, glass, or basalt [4] bundled into yarns, is usually configured into a mesh that interlocks with the matrix in the composite. Basalt textiles have recently received growing attention due to their natural origins, enhanced durability, heat resistance, and superior strength and stiffness compared to materials like E-glass fibres [5,6]. The existing knowledge on the performance of TRC systems made of these textiles is still limited.

The pursuit of manufacturing load-bearing structural components from TRC is expected to be mainly governed by the serviceability limit state conditions (i.e. cracking and excessive deflections under service

loads [7]). A solution for improving the service response of TRC-based components is to prestress the textile reinforcements. The existing, but limited literature on this topic shows that prestressing of textiles can enhance the composite tensile behaviour, cracking strength, flexural strength and toughness [7–9]. Yet, the effectiveness of this method relies heavily on the bonding interaction between the matrix and the reinforcement. In the prestressing process, once the tensioned textile is released into the hardened matrix, it attempts to revert to its original length. The surrounding concrete resists this natural tendency through bond and mechanical interlocking. In this context, the bond between the textile reinforcement and the matrix is one of the primary mechanisms influencing short- and long-term deformations. Moreover, the interfacial bond behaviour is a critical factor in determining the structural response of TRC composites in terms of strength, crack distribution, ductility, absorbed energy and, ultimately, the failure mode [10,11]. Enhancing the interfacial bond can mitigate stress localisation during crack propagation and promote a more uniform distribution of cracks [12], thus improving load-bearing capacity [13]. Moreover, the failure mode at the ultimate limit state is predominantly governed by bond strength, which

\* Corresponding author.

E-mail addresses: [mohammed.hutaibat@nottingham.ac.uk](mailto:mohammed.hutaibat@nottingham.ac.uk) (M. Hutaibat), [b.ghiassi@bham.ac.uk](mailto:b.ghiassi@bham.ac.uk) (B. Ghiassi), [walid.tizani@nottingham.ac.uk](mailto:walid.tizani@nottingham.ac.uk) (W. Tizani).

<https://doi.org/10.1016/j.conbuildmat.2024.137309>

Received 23 April 2024; Received in revised form 18 June 2024; Accepted 1 July 2024

Available online 4 July 2024

0950-0618/© 2024 The Author(s). Published by Elsevier Ltd. This is an open access article under the CC BY license (<http://creativecommons.org/licenses/by/4.0/>).

may involve textile slippage, rupture, or delamination depending on the bonding strength with the surrounding matrix [14,15].

The textile-to-concrete bond behaviour has been the subject of several studies in the literature, examining the influence of mechanical properties of constituent materials, such as matrix properties (e.g., strength and shrinkage), textile properties (e.g. type, geometry, coating) [9,16–20], or manufacturing method [21–23]. Research on the bond behaviour of prestressed textile-reinforced concrete has, however, been very scarce. Recently, the studies conducted by Krüger [16,24] and Shilang Xu [25,26] examined the influence of prestressing (within a range of 10–23 % prestress levels) on the bond behaviour of one-day-cycle produced samples (i.e. the prestressed textile was released after 1-day of concrete curing). These investigations also evaluated the impact of epoxy coating on the bond behaviour of textiles made of carbon (prestressed up to 23 %), aramid (prestressed up to 16 %) and AR-glass (prestressed up to 20 %). Prestressing dry carbon fibres resulted in a consistent increase in the pull-out load, regardless of variations in the prestress level, attributed to the realignment and bundling of the inner filaments due to their slippage upon release, thereby increasing their contact zones and sliding friction. However, it was observed that the adhesive bond of the used dry carbon was relatively weak, resulting in decreased stiffness values at high prestress levels due to insufficient bonding at the time of release, while stiffness increased at low prestress levels [25]. Furthermore, the realignment of inner filaments and the matrix's inability to penetrate the dense carbon fibres can result in immediate relief of transverse pressure from prestressing, making prestressing unsuitable for this type of reinforcement [16]. This inner action can be mitigated by impregnation; prestressing resin-impregnated textiles, such as carbon and aramid, showed a more pronounced enhancement of the initial stiffness, bond strength, and friction due to the transverse pressure created by prestressing. Additionally, prestressing of textile reinforcement reduced deflection at crossing points between weft and warp yarns, thereby increasing bond strength through increased transverse compressive stresses. Compared to carbon, this effect was particularly notable in aramid (woven fabric). Their studies highlighted the importance of carefully selecting resins with high modulus of elasticity and shear modulus to optimise prestressing efficiency. However, practical limitations were observed with AR-glass textiles, including issues like creep and low static fatigue limit. Investigations on the bond behaviour in basalt-based TRCs (BTRCs), however, remain unaddressed.

To address the above, this study is aimed at studying the effect of prestressing on the bond behaviour of Basalt Textile reinforcement. For this, a one-sided pull-out test set-up has been modified and presented to study the bond behaviour of both prestressed and non-prestressed samples. Tests have been conducted on non-prestressed samples over an embedment length range of 30–50 mm to assess the bond capacity, failure pattern, and optimal embedded length for prestressed samples. Prestressed samples were then prepared only at one embedded length to investigate the influence of prestress level (0 %, 13 % and 35 %), release time (1-day and 7-day) and testing age (28 and 90 days) on the bond behaviour of BTRCs. Finally, the obtained experimental data are used to draw indications on the effect of prestressing on the saturated crack spacing of TRC composites.

## 2. Experimental programme

### 2.1. Mix composition and material properties

A high-strength concrete with sufficient flowability (self-compacting) and high early strength was designed and implemented in this study (Table 1). The mix comprises rapid-hardening cement (CEM I 52.5 R), fly ash, and a small amount of silica fume. Specifically, 57.5 % of the developed mix comprises sand, achieving a sand/binder ratio of 1.35. The maximum particle size of sand is 1 mm to ensure full matrix coverage around the textile yarns. The workability of the fresh concrete was determined using the mini-slump cone method, with an average

**Table 1**

Mix proportions and mechanical properties of the cementitious binder.

Materials/Properties	Value
Cement (52.5 R)* [Kg/m <sup>3</sup> ]	589.2
Fly Ash [Kg/m <sup>3</sup> ]	189.0
Silica Fume [Kg/m <sup>3</sup> ]	50.3
Sand 0.6–1.0 [Kg/m <sup>3</sup> ]	1121.6
Water [Kg/m <sup>3</sup> ]	259.2
Superplasticiser dosage [Kg/m <sup>3</sup> ]	13
Slump [mm]	280
1-day compressive strength** [MPa]	29 (5.7)
7-day compressive strength** [MPa]	65 (6.9)
28-day compressive strength** [MPa] (Cubes)	113 (5.1)
28-day compressive strength** [MPa] (Cylinders)	104 (7.55)
90-day compressive strength** [MPa]	116 (6.3)
Flexural strength [MPa]	11.25

\* CEMI Rapid hardening concrete. \*\*Compressive strength of concrete is based on samples cured under water. The result's coefficient of variation is presented in parentheses.

spread of 280 mm. Compressive strength of the mortar was determined according to ASTM C109 [27] on three identical 50 mm-sized cubes at different ages (1, 7, 28 and 90 days) with a load rate of 1.5 kN/s and using a 200 kN servo-controlled universal testing machine. Additionally, compressive tests were performed on cylinders as per EN 12390–3 [28], with a non-standard size of 50 mm in diameter and 100 mm in height, justified by taking into consideration the maximum aggregate size (<1 mm), and employing a load rate of 1.18 kN/s. The flexural strength of the matrix was evaluated as per EN1015–11 [29] on three prismatic specimens measuring 40x40x160 mm<sup>3</sup>.

A basalt-based textile grid with the characteristics detailed in Table 2, as provided in the manufacturer's datasheet, was used as the reinforcement. The weft (horizontal) and warp (vertical) yarns are evenly spaced to create a bidirectional mesh with dimensions of 25×25 mm. The experimental tensile strength and elastic modulus of each yarn were 1356 MPa (COV = 4.0 %) and 81 GPa (COV = 4.78 %), respectively, following the methodology outlined by Hutaibat et al. [23]. This evaluation involved bare textile coupons measuring 410 mm in length and 50 mm in width tested using an Instron machine at a controlled displacement rate of 0.005 mm/s.

### 2.2. Test specimens and investigated parameters

The bond performance of prestressed and non-prestressed basalt textile reinforced concrete was investigated using single-yarn pull-out tests [30–33]. The testing programme was structured into two stages; at least five specimens were tested for each investigated parameter, with 80 samples. In the initial stage, a range of embedment lengths were investigated for the subsequent evaluation of the representative bond behaviour response. This preliminary investigation sought to establish the optimal embedded length for non-prestressed specimens, and ensuring to obtain yarn slippage failure mode, considering the unique characteristics of textile reinforcement [34]. These included three distinct embedment lengths of 30, 40 and 50 mm. After analysis of the results obtained from this stage, a 40 mm embedded length was selected to prepare prestressed samples. This choice was made considering any potential improvements in bond performance and, therefore, avoiding any pull-out rupture in prestressed samples.

In the second stage, two sets of samples were prepared and classified based on their prestress release time (i.e. 1-day and 7-day). The selection of a 1-day release time was driven by the practical need to enable a 1-day cycle production, to ensure the feasibility and successful application of prestressed textile structures into industrial applications. This choice aligns with the industry practices (typically 1–4 days) and aims to investigate the effect of time-dependent material properties, considering that no accelerated curing was adopted in this study. The matrix used was designed to adhere to prestressed structures code requirements (ACI

**Table 2**  
Mechanical properties of basalt textile (Manufactures' Data).

Material	Coating	Fibre orientation	Mesh size	Modulus of elasticity	Weight	Density	Nominal thickness
			[mm]	[GPa]	[g/m <sup>2</sup> ]	[g/cm <sup>3</sup> ]	[mm]
Basalt	Polymer	Bidirectional	25×25	89	220	2.67	0.037

318–95 and 1996 AASHTO LRFD) so that the selected prestress force is less than 0.6 times the specified compressive strength at the time of release (i.e.,  $0.6 f_c'$ ) [35,36]. This also replicated our previous experimental results on the bending performance of prestressed TRC plates prepared with the same materials [7]. Within each set, two levels of prestress were applied, purposely set at 13 % and 35 % of the ultimate tensile strength of the textile material. The choice of 35 % maximum prestressing level falls just below the ACI recommendations for FRP tendons, which typically range between 40 % and 65 % for aramid and carbon FRP tendons [7,37]. Additionally, basalt FRP bars have been found to endure a creep rupture stress when loaded up to 50 % of their tensile strength [38]. This indicates the maximum stress level considered in this study should be far from creep rupture stresses, although this should be validated in future studies. This choice (i.e. 35 % maximum prestress level), therefore, considers variations in the bond behaviour, interfilament stress transfer between textile reinforcement and FRP tendons, and safety considerations to achieve a balanced approach between performance and material suitability [7]. Furthermore, these configurations were tested at two ageing intervals (i.e. 28 and 90 days) to investigate the potential changes in the bond behaviour due to the combined effect of concrete hydration and prestress losses.

The nomenclature for the investigated samples is expressed through the notation  $xPxRxLBY$ , where the letter  $x$  quantifies the numerical value of each parameter. Specifically,  $P$  denotes the level of applied prestressing,  $R$  represents the time before prestressing release,  $D$  indicates the age at which the samples were tested, and  $L$  stands for the length of the embedded yarn.  $BY$  identifies control samples lacking a release time at the end of the notation.  $B1$  and  $B7$  correspond to the 1-day and 7-day release times, respectively (Table 3).

**2.3. Sample preparation**

Fig. 1 illustrates a schematic representation of the specimens. The samples are designed with a square geometry to simplify the testing procedure and to ensure proper yarn alignment. The specimens' configuration consists of two separate main sections: the upper (grip) and the lower sections (sample). Both sections are made of a concrete matrix, with a single yarn embedded longitudinally across both components. This design avoids potential complications associated with using epoxy resin as a gripping method while maintaining a setup

**Table 3**  
Tested specimens.

Test Age	Sample ID	Embedment length (L) [mm]	Prestress level [%]	Prestress release time [day]
28 days	0P0R28D30L	30	0	-
	0P0R28D40LB1	40	0	-
	0P0R28D50L	50	0	-
	13P1R28D40L	40	13	1
	35P1R28D40L	40	35	1
	0P0R28D40LB7	40	0	-
	13P7R28D40L	40	13	7
	35P7R28D40L	40	35	7
	90 days	0P0R90D40LB1	40	0
13P1R90D40L		40	13	1
35P1R90D40L		40	35	1
0P0R90D40LB7		40	0	-
13P7R90D40L		40	13	7
35P7R90D40L		40	35	7

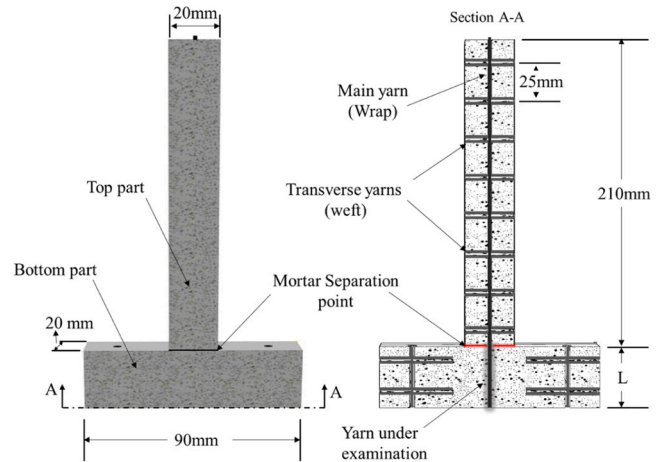


**Fig. 1.** Representative cross-section of the pull-out sample.

comparable to the established one-sided pull-out configuration. This will ensure that the tensile force is transmitted to the textile yarn through the concrete. The bottom section, which represents the part under examination, has dimensions of 90 mm in width, 20 mm in thickness, and a length matching the embedment length ( $L$ ) (see Fig. 1). On the other hand, the top section is incorporated to grip the samples securely. It measures 20 mm in width and thickness, with a length of 210 mm (anchorage length), to ensure sufficient gripping capacity and to prevent potential yarn slippage.

The preparation of all tested specimens was carried out in two distinct stages (Fig. 2). Initially, the bottom part was cast, followed by the top part (the grip). Separate moulds were utilised for each stage in both prestressed and non-prestressed samples. The textile was positioned within the mould and secured using steel dividers for non-prestressed specimens to achieve the desired configuration. The embedment length was controlled using polystyrene plies of varying lengths. Transverse yarns were cut at the sample's centre, so a singular yarn is being examined. Subsequently, concrete was poured into the mould and allowed to harden for 24 hours. Afterwards, the samples were demoulded and submerged in water for a 7-day curing period. The cured samples were placed in the second mould to cast the top part, with a thin insulation tape (0.15 mm thick) separating both parts. The samples were then stored in a controlled temperature curing room until the day of testing.

Prestressed specimens followed a similar preparation process. However, to apply the desired prestressing force, a specialised prestressing rig developed by the authors in a previous study (as shown in Fig. 2) was employed [7]. This rig was designed to apply a uniform tensile force across the textile. After securing the textile in the clamps, the load was applied using a hydraulic jack, with load control facilitated by a load cell. Once the desired load level was achieved, the same procedure as for non-prestressed samples was followed for casting the bottom part of the samples. The load was released after reaching the desired release time, and the samples were removed from the rig and demoulded (Fig. 2). As mentioned above, curing conditions similar to those of non-prestressed samples were maintained for the bottom part of the samples. In contrast, the top part was cast following the same procedure as in the non-prestressed samples. That is, prestressing is only

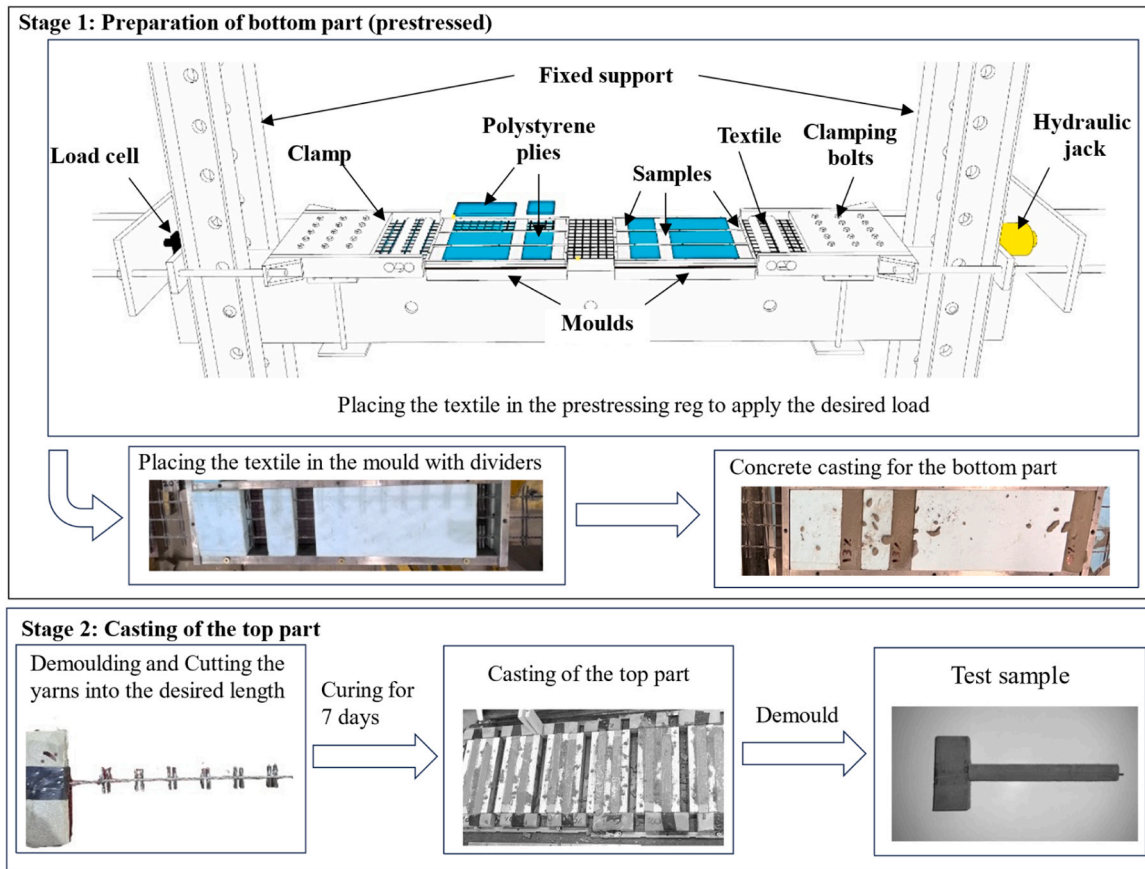


Fig. 2. Preparation stages of pull-out samples: Stage 1) Prestressing rig and casting of the bottom part; Stage 2) Casting of the top part.

applied to the part under examination (bottom part).

2.4. Pull-out test setup

Two primary test configurations commonly used for pull-out tests are single-sided pull-out tests [18,23,30,31,33,39] and double-sided pull-out tests [16,30,40]. In the single-sided tests, a yarn is embedded at one end within the concrete matrix and left unbonded at the other end. The tensile force is applied to the free length of the yarn either directly by the machine grip or through an epoxy resin block. Utilisation of the epoxy block can minimise any possible damage to the filaments and provide a uniform stress distribution across the tested yarn [18,32,33]. Generally, one-sided pull-out testing is preferred for its simplicity and relatively low variations over the obtained results but can provide lower values compared to double-sided tests [30]. Conversely, in the two-sided tests, whether with symmetrical or asymmetrical anchorage lengths, the yarn is embedded in concrete at both sides, with the pull-out force being transferred to the yarns through the concrete with both sides in tension. This method yields higher peak load values due to the mortar’s contribution to the tensile load resistance [30]. The test setup developed in this study follows the principles of a one-sided pull-push setup [30,31, 41].

Fig. 3 illustrates the designed setup for the pull-out test. The load was applied using a Zwick Roell testing machine under displacement control set at a 1 mm/min load rate [33]. Each part was placed in a special clamp to ensure a sufficient grip over the specimens. In this configuration, the bottom part of the sample was held in place within a hollow steel frame, implying pressure from both sides. The top part was clamped using two steel plates, exerting tension through gripping. Both parts were firmly secured within the testing machine grip using steel rods with a radius of 30 mm to create a pull-push mechanism for applying the

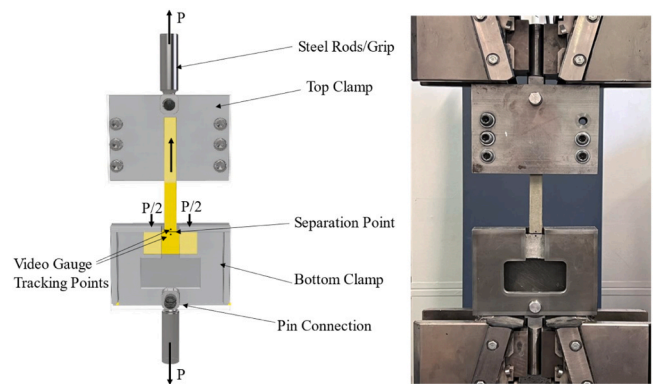


Fig. 3. Pull-out test schematic setup.

pull-out load. A non-contact measurement method for monitoring the displacement was used for accurate measurements, using a high-precision video gauge extensometer with an accuracy of 0.05 μm (over a 25 mm measurement range). For this purpose, two tracking points were marked on the samples’ ends at the separation point (see Fig. 3). The distance between these tracking points was as little as 5 mm, ensuring sufficient accuracy and that the measured displacement data were solely representative of the pull-out behaviour and not influenced by any other material deformations or elongation during the test.

The bond stiffness ( $\kappa$ ) was calculated as the slope of the linear portion of the load-slip curves. To determine the average maximum bond stress ( $\tau_{max}$ ) and frictional stress ( $\tau_f$ ), the relative pull-out peak load values (P) extracted from the experimental data were divided by the nominal contact surface of the embedded yarn as expressed by the equation  $\tau =$



$P/\pi\Phi L$ , where  $\Phi$  represents the nominal diameter of the yarn. For calculating the nominal diameter or the perimeter of the yarns, both nominal thickness and images taken using a microscope are utilised, and the differences are discussed. The debonding energy is assessed by quantifying the area under the load-slip curve up to the peak load, employing the trapezoidal rule. This evaluation serves as an indication of the adhesion bond's quality, as it measures the amount of energy dissipated during the separation of the yarn from the matrix, encompassing both elastic stretching and complete debonding. Additionally, the pull-out energy, presenting the dissipated energy by the frictional interface between the yarn and the matrix during the pull-out [42], is determined in a similar way to debonding energy. However, it encompasses the region beyond the peak load point and extends up to a 10 mm slip for ease of comparison, providing further insights into the frictional bond characteristics.

### 3. Results and discussion

#### 3.1. Yarns cross-section area

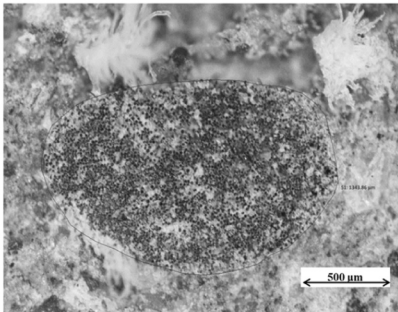
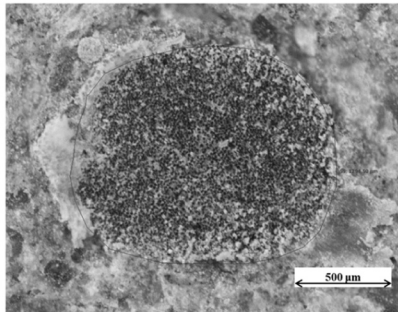
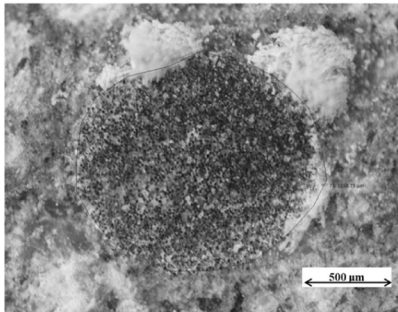
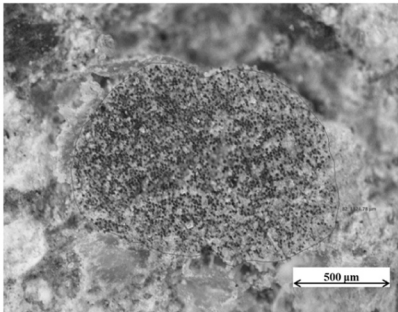
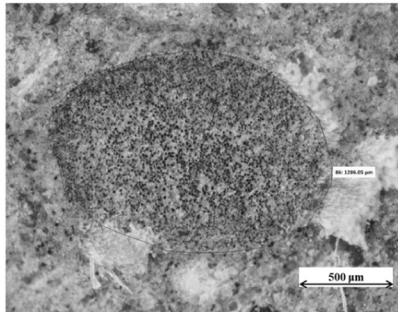
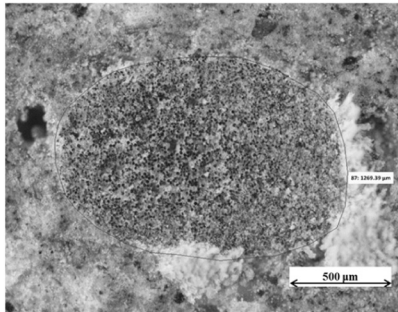
The microscope images depicting area measurements on thin sections of the samples, presented in Table 4, clearly show that prestressing has influenced the measured area. These measurements indicate a decrease of 2.3 % and 3.8 % at prestress levels of 13 % and 35 %, respectively. This reduction is attributed to the tensioning of the filaments and Poisson's effect during prestressing, resulting in fewer voids and closer filament contact as the prestress level rises. Additionally, the shape of non-prestressed yarns, as shown in B1 and B7, exhibited some non-uniformity, whereas prestressed yarns tend to adopt a more uniform, circular form.

#### 3.2. Summary of pull-out results

Pull-out samples exhibited a typical load-slip behaviour in both prestressed and non-prestressed samples; see Fig.(4) for an idealised response. This response results from two main mechanisms - adhesion and friction - and can be divided into three stages. In stage IA, the yarn is completely bonded to the matrix, controlled mainly by the adhesive bond between the matrix and the yarn. This adhesive bond results from a chemical reaction between the fresh concrete and the textile surface. In the case of prestressed samples, the applied stress initially causes a reduction in the diameter of the textile roving, as shown in the microscopic measurements, due to Poisson's effect. Consequently, when released, the stresses are transferred into the matrix over a certain length called the transfer length (the length from the end of the sample where the yarn stress is zero to the point where the prestressing is fully effective [43]). As the released yarns undergo lateral expansion, they generate a compressive force on the surrounding concrete. Depending on the Poisson's ratio, this compressive force is countered by the radial pressure from the hardened concrete, known as the Hoyer effect [44]. This contraction of the yarn will create a wedge at the end of the sample, which is anticipated to increase the bond strength further by increasing the mechanical friction at this stage. Key parameters such as the matrix strength and prestress level can influence the extent of this bond strength enhancement by affecting the anchorage length required to transfer the applied prestress stresses effectively [45,46].

On a global level, this directly influences the structures' cracking behaviour regarding crack spacing and width and their ultimate deflections and failure mechanism. Increasing the bond strength can result in denser cracks and low deflections, leading to filament rupture as the primary failure mode. In contrast, lower bonding strength tends to have the opposite effect on the cracking behaviour, with filaments slipping as the predominant failure mechanism.

**Table 4**  
Microscope measurements on thin sections.

<b>0PB1</b>	<b>13P1R</b>	<b>35P1R</b>
		
Area: 1.34 mm <sup>2</sup> Diameter: 1.31 mm	Area: 1.29 mm <sup>2</sup> Diameter: 1.28 mm	Area: 1.26 mm <sup>2</sup> Diameter: 1.27 mm
<b>0PB7</b>	<b>13P7R</b>	<b>35P7R</b>
		
Area: 1.32 mm <sup>2</sup> Diameter: 1.30 mm	Area: 1.29 mm <sup>2</sup> Diameter: 1.28 mm	Area: 1.27 mm <sup>2</sup> Diameter: 1.27 mm

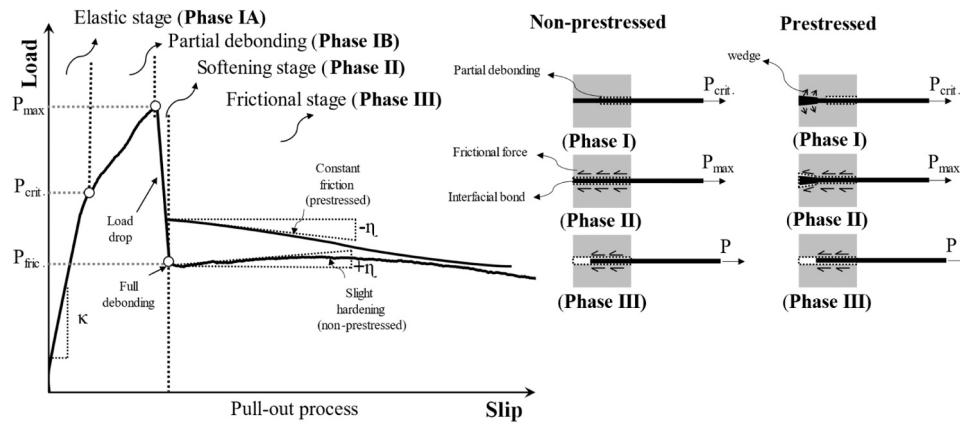


Fig. 4. Idealised Load-slip curve of the pull-out test results.

Under increasing the load, the sample undergoes a linear increase in the pull-out load (and interface shear stresses) with a corresponding slip. Once the load reaches a critical value ( $P_{crit.}$ ), yarn debonding at the loaded end initiates (Stage IB). In this stage, the total pull-out load is resisted by two mechanisms: the cohesive bond in the bonded regions and the frictional bond in the unbonded regions. This is associated with decreased bond stiffness with respect to Stage IA. With increasing the pull-out load at this stage, the length of the debonded region increases until a full debonding occurs along the embedded length. This usually can be concurrent with reaching the peak pull-out load ( $P_{max}$ ) [30,33]. After this, a softening response (Stage II) with a sudden drop of the load or a smooth transition, depending on the frictional strength of the system, is observed. In the experimental tests conducted in this study, a drop in the pull-out load was observed after reaching the peak, indicating a higher cohesive bond strength than a frictional bond. The load drop after the peak load (indicates a transition from a combined

chemical and frictional bond to a pure frictional bond) and is more significant when the frictional force is much smaller than the chemical bond [47,48], as is the case of this study. This stage is followed by a consistent slip response with a slight hardening (stage III), represented by a positive frictional slope value ( $\eta$ ), gradually decreasing with the reduction in the embedded length of the yarn as it pulls out [49]. Here, the frictional bond serves as the sole resisting mechanism, which increases in the form of a slight hardening due to the abrasion and jamming effect between the yarn surface and the surrounding matrix [33, 50,51]. However, a nearly constant friction behaviour was observed in prestressed samples, indicated by the negative values of the hardening slope ( $\eta$ ). Nonetheless, the frictional stresses remained higher than those observed in the non-prestressed samples. This increase can be attributed to the Poisson's ratio effect on the frictional bond becoming more dominant than the jamming effect, mentioned previously.

Table 5 summarises the experimental results, which are discussed in

Table 5  
Summary of the pull-out test results.

Age	Sample ID	Initial stiffness ( $\kappa$ ) [N/mm]	Peak Load ( $P_{max}$ ) [N]	Maximum stress ( $\tau_{max}$ ) [MPa]	Slip @peak load [mm]	Debonding energy [N.mm]	Frictional Load ( $P_{fric.}$ ) [N]	Frictional Slope ( $\eta$ ) [N/mm]	Frictional stress ( $\tau_f$ ) [MPa]	Pull-out energy [N.mm]	
28 days	0P0R28D30L	893 (14.5)	458 (10.4)	3.71 (10.4)	0.41 (30.0)	132 (28.2)	165.7 (22.7)	9.91 (36.6)	1.34 (22.7)	1116 (22.7)	
	0P0R28D40L1	1039 (28.4)	545 (2.2)	3.31 (2.2)	0.60 (36.0)	222 (24.8)	214.5 (13.4)	18.94 (63.1)	1.31 (13.4)	1465 (19.1)	
	0P0R28D50L	1189 (16.6)	620 (6.1)	3.02 (6.1)	0.79 (14.1)	349 (11.6)	275.4 (8.4)	33.1 (42.1)	1.34 (8.4)	1937 (16.0)	
	13P1R28D40L	1293 (12.6)	520 (5.5)	3.23 (5.5)	0.45 (45.7)	155 (46.6)	302.3 (22.1)	-33.5 (-27.4)	1.88 (22.1)	1655 (22.1)	
	35P1R28D40L	985 (28.8)	281 (11.7)	1.75 (10.3)	0.27 (68.8)	53 (75.4)	242.8 (5.5)	-13.25 (-26.4)	1.52 (5.5)	1318 (5.8)	
	0P0R28D40LB7	1010 (19.7)	540 (3.3)	3.32 (3.28)	0.64 (27.4)	228 (21.8)	235.6 (7.4)	20.3 (33.2)	1.45 (7.4)	1601 (17.0)	
	13P7R28D40L	1341 (20.1)	634 (8.3)	3.94 (8.30)	0.55 (32.2)	251 (31.6)	326.0 (20.4)	-44.8 (-21.8)	2.02 (20.4)	1703 (33.1)	
	35P7R28D40L	1003 (15.6)	630 (11.0)	3.95 (11.0)	0.76 (40.7)	307 (46.2)	341.8 (14.6)	-37.9 (-18.1)	2.14 (14.6)	1956 (17.4)	
	90 days	0P0R90D40L1	1003 (9.4)	566 (6.1)	3.44 (6.07)	0.64 (8.7)	265 (16.1)	236.4 (11.0)	32.3 (29.2)	1.44 (11.0)	1474 (6.2)
		13P1R90D40L	1286 (13.4)	508 (6.4)	3.16 (6.36)	0.51 (42.7)	164 (49.2)	315.8 (17.1)	-36.8 (-72.5)	1.96 (17.1)	1555 (12.6)
35P1R90D40L		1009 (9.8)	366 (10.6)	2.29 (10.6)	0.34 (29.9)	89 (35.6)	279.2 (9.0)	21.4 (63.8)	1.75 (9.0)	1662 (13.2)	
0P0R90D40LB7		1076 (12.5)	540 (9.8)	3.32 (9.78)	0.47 (31.4)	177 (32.5)	287.3 (21.8)	27.9 (-39.8)	1.77 (21.8)	1818 (29.7)	
13P7R90D40L		1366 (17.6)	680 (8.7)	4.22 (8.65)	0.53 (37.9)	251 (50.6)	382.2 (22.8)	-18.6 (-61.8)	2.37 (22.8)	2119 (31.9)	
35P7R90D40L		1400 (24.8)	566 (14.6)	3.55 (14.6)	0.50 (43.2)	201 (48.6)	340.7 (24.4)	-28.5 (-66.3)	2.13 (24.4)	1805 (29.2)	

The result's coefficient of variation is presented in parentheses.

the following sections. It should be noted that in these results the frictional stress is calculated using the calculated cross-section area of the yarns using microscopic images as discussed in the previous section.

### 3.3. Pull-out response of non-prestressed samples

Fig. 5 illustrates the load-slip responses obtained from the yarn-to-concrete bond tests on samples with different embedment lengths. The samples' common failure mode at all the selected embedment lengths was characterised by a complete pulling out of yarns, with abrasion of the surface coating and the surface threads of the yarn, without any rupture for the selected range of embedment lengths (Fig. 6a,b,c). Upon reviewing (Table 5), it's evident that the recorded pull-out load values for the same sample set align closely within an acceptable range (max COV = 10.4 %). A constant increase over the bond peak load, debonding energy and slip at peak load with increasing the embedment length can be observed in Fig. 5 and Table 5. Among the non-prestressed samples, the highest average peak load was measured at 620 N for an embedment length of 50 mm (with COV = 6.11 %). This represents a 14 % increase compared to the 40 mm samples and a 35 % increase compared to the 30 mm samples. However, when the pull-out resistance values are normalised into average bond stress (i.e. dividing the peak load to the embedded length – note this assumes a uniform distribution of shear stresses which is more accurate in short embedded lengths), the 50 mm samples exhibit a 19 % decrease, and the 40 mm samples show an 11 % decrease in the maximum bond stress ( $\tau_{max}$ ) compared to the 30 mm samples.

The post-peak behaviour (Stage III) of the samples exhibited an increase in the resisting frictional force (i.e.  $P_{fric}$  in Fig. 4) and pull-out energy (calculated until the peak load) with increasing the embedded length, as expected. However, it was observed that the embedded length had no significant effect on the stress component of friction, i.e.  $\tau_f$  as indicated by the nearly constant average frictional stress values reported in Table 5. Moreover, the slight slip-hardening response reported above was more notable in samples with longer embedded lengths. The primary cause of slip-hardening in polymer-impregnated yarns, as mentioned previously, is abrasion of the yarn's coating surface due to its interaction with the matrix during the pull-out process; this occurs when the relatively low hardness of the surface coating/knitting threads yarn's surface abrades against the rougher cement matrix when pull-out, resulting in the accumulation of fibre debris and a jamming effect that increases the interface shear stress. An increase in shear stresses is also expected with slip increment in the frictional stage, especially with longer embedment lengths, which leave more fibre scrapings at the debonded interface (see Fig. 6d) [33,50,51]. The role of yarn surface geometry on the slip-hardening response remains unknown, but it is expected that this can play a role (i.e. surface with higher roughness are

expected to have increased frictional resistance, which also increased the risk of abrasion).

### 3.4. Effect of prestressing level and release time

Prestressed samples exhibited a comparable failure mode to that observed in non-prestressed samples of identical embedded length (i.e., 40 mm). The typical experimental load-slip curves of the prestressed samples are presented in Fig. 7, with the results summarised in Fig. 8. The load-slip curves illustrate a change in the pull-out response with increasing the prestressing load levels or release times (see Fig. 7a, b, c). An enhancement in the pull-out response is evident at prolonged release durations. The influence of prestressing on the pull-out resistance during the post-peak stage (Phase III) appears positive, except for the 1-day release samples at 35 % prestress level (i.e. 35P1R28D40L), which show a deterioration in the bond performance. This refinement in the post-peak stage is attributed to the increased frictional force caused by the lateral expansion and the resulting Poisson ratio effect of the released prestressed yarns.

In the 1-day release samples, the bond's initial stiffness ( $\kappa$ ) (Fig. 8a) increased by 25 % in samples subjected to a 13 % prestress level compared to the non-prestressed samples. However, at a higher prestress level of 35 %, the stiffness decreased and became comparable to control non-prestressed samples (OPOR28D40LB1), showing a 5 % decrease. Similarly, in the 7-day release samples, a comparable trend can be observed, with a slightly higher increase in stiffness (28 %) at the prestress level of 13 % when compared to their non-prestressed counterparts (i.e. OPOR28D40LB7). Both release times had almost the same stiffness values at a 35 % prestress level. This indicates the consistent impact of high prestress levels on the initial stiffness despite the change in release time of the samples.

The prestressing effect on the peak pull-out load and maximum bond stress ( $\tau_{max}$ ) was found also to be dependent on the release time (see Fig. 8b, c). In 1-day release samples, compared to non-prestressed samples (OPOR28D40LB1), there was minimal change in the peak load and strength at a 13 % prestress level, with only a 5 % and 2 % decrease, respectively. However, a more substantial reduction of 48.4 % in the peak load and 47 % in the maximum bond stress was noted at a 35 % prestress level. This outcome can be attributed to the disruption of the adhesive bond between the textile roving and the matrix, mainly when the prestress is released when the matrix is still premature and the bond has not fully developed, resulting in the yarns being pulled into the matrix. As a result, the adhesive bond fails to form fully, leaving only friction to counter the applied load effectively, which ultimately leads to the observed reduction in bond strength. This disruption is intensified with the increase in the internal stresses on the material caused by higher prestress levels. It's worth noting that's the difference between

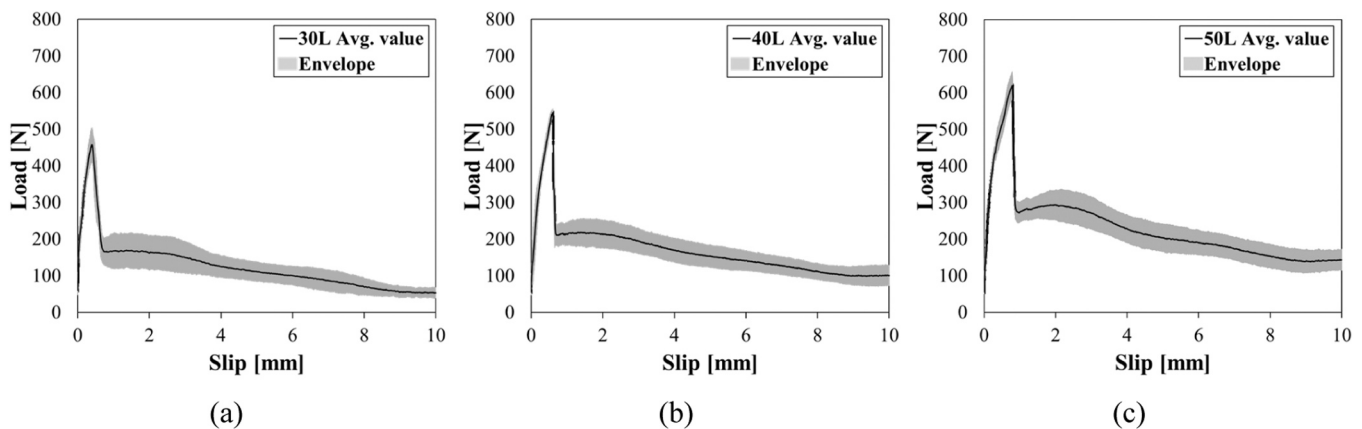


Fig. 5. Load-slip response at different embedment lengths: a) 30 mm embedment length (30 L) samples; b) 40 mm embedment length (40 L) samples; c) 50 mm embedment length (50 L) samples.



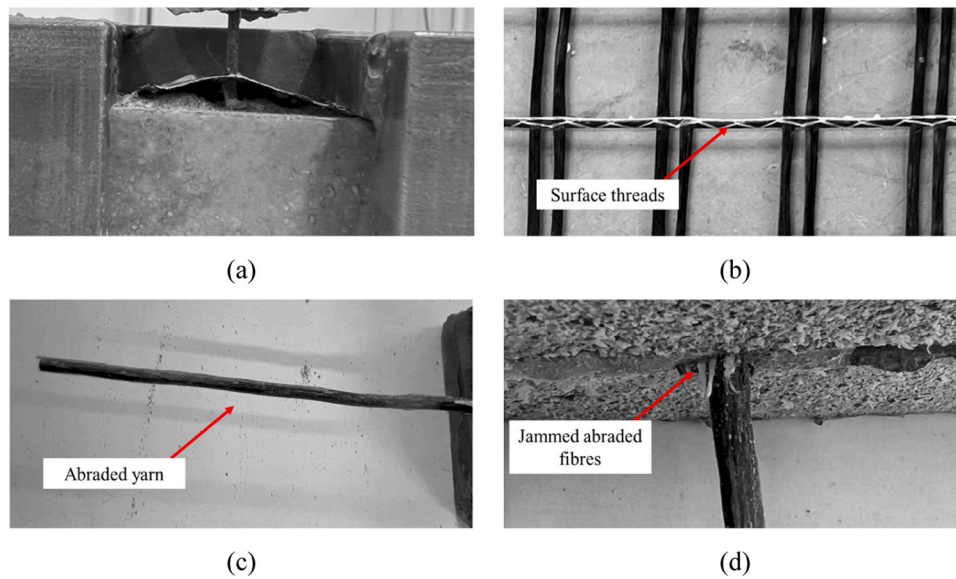


Fig. 6. Pull-out process of the samples: a) Yarn pull out at the specified point; b) Original shape of the yarn; c) Failure mode of the yarn (complete pull out with surface abrasion); d) Abraded fibres jamming effect.

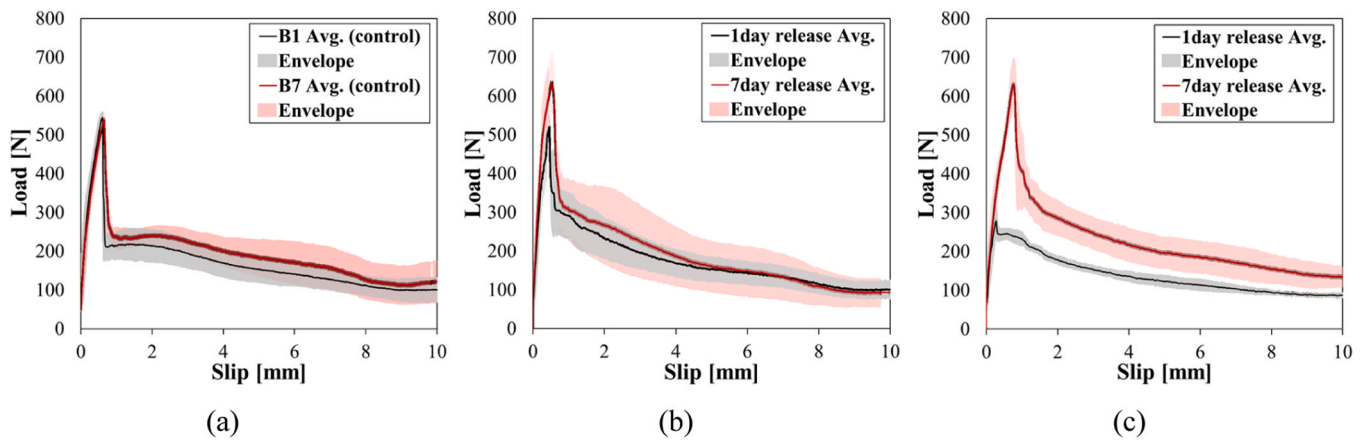


Fig. 7. Effect of prestressing level and release time: load-slip curves of 1-day (1R) and 7-day (7 R) release samples (at 28 days of age): a) Control samples; b) 13 % prestress samples; c) 35 % prestressed samples.

the peak load values and bond strength is a result of the variation in the yarn area caused by prestressing level used for calculating the bond strength.

In contrast, for the 7-day prestressed samples, the yarn exhibited increased resistance to the pull-out load. The prolonged release time allowed for the development of sufficient bond strength to effectively resist applied prestress forces and develop a significant Poisson effect, resulting in a noticeable enhancement of bond peak load. However, for the 7-day release time, both prestress levels (i.e. 13 % and 35 %) exhibited nearly equivalent values regarding the pull-out peak load and bond strength with a 17.4 % increase over the non-prestressed samples. The extended-release period facilitated the establishment of adequate adhesion between the matrix and the textile roving regardless of the prestress level. Compared to non-prestressed samples (OPOR28D40LB7), frictional stress was remarkably influenced by both prestressing level and release time (Fig. 8d). A substantial increase of 43 % in frictional force was observed in the 13 % prestress samples when released after 1-day, whereas this effect became less pronounced with only a 16 % increase in samples prestressed at 35 %. However, the extended-release time did not significantly affect the average frictional stress at low prestress levels, as the prestress influence remained constant over the

13 % prestress level samples, showing a consistent 39 % increase. Conversely, its positive impact became evident in the 35 % prestressed samples, where the average frictional stress increased substantially by 48 %. While higher frictional forces are supposed to increase the bond strength at higher prestress levels, the bond strength was not affected beyond a certain limit, this can be attributed to the fact that the frictional force is not the only resisting mechanism in the bond strength. The chemical bond exceeds the frictional force for the materials used in this experiment, as both prestress levels resulted in the same strength. Other factors may also influence prestressing at a higher level, such as the transfer length. Higher prestress levels require longer anchorage lengths, and this suggests that additional damage from higher prestress levels may still affect the bond, although to a lesser degree compared to the 1-day release time.

Furthermore, the influence of prestressing on debonding energy values at the peak load was substantial (Fig. 8e). In comparison to non-prestressed samples, the 1-day release samples showed a prominent and progressively more pronounced decrease as the prestress level increased. Specifically, a significant decrease of 30 % and an even more substantial 76 % reduction was observed at 13 % and 35 % prestress levels, respectively. This reduction in 13 % prestressed samples was a



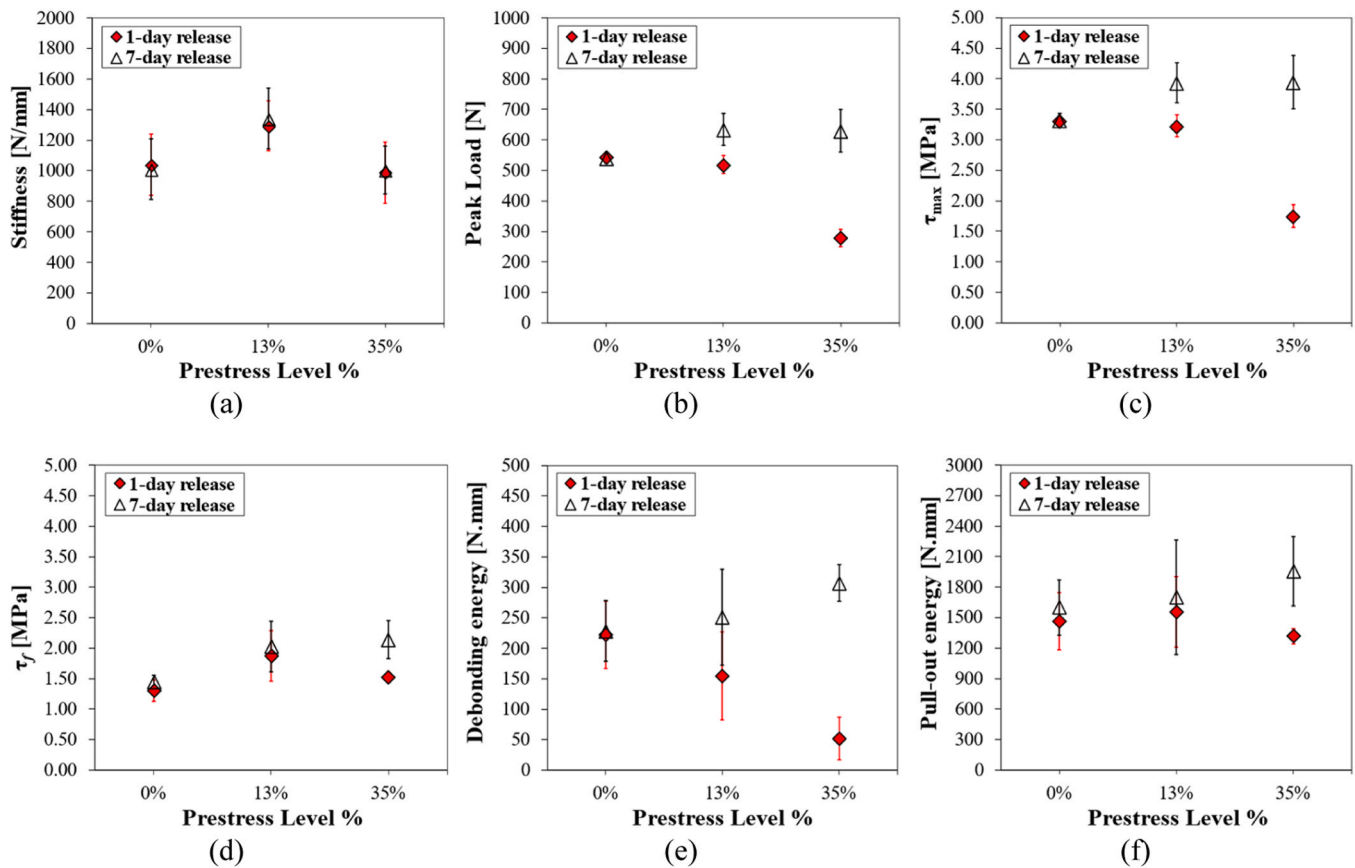


**Fig. 8.** Effect of prestressing level and release time at 28 days of age on: a) Initial stiffness; b) Peak load; c) Maximum Stress; d) Frictional stress; e) Debonding energy at peak load; and f) Pull-out energy.

result of the increased stiffness, while the destruction of the bond strength at higher prestress levels (i.e., 35 %) accounted for a larger reduction. In contrast, the 7-day released samples exhibited a variant behaviour. Debonding energy values increased by 10 % at a low prestress level (i.e., 13 %) and displayed an even more significant increase of 34 % at a higher prestress level of 35 % over their control samples. This underlines the advantageous influence of prolonged-release times on the sample's debonding energy, particularly at elevated prestress levels, caused by the reduced stiffness but the consistent peak load in those samples. An increase of 13.7 % in the pull-out energy caused by the increased frictional load (Fig. 8f) was observed in the 13 % prestress samples (13P1R28D40L) when released after 1 day, contrasting with a 10 % decrease at a higher prestress level of 35 % compared to 0P1R28D40LB1 samples. Despite the increased frictional load stated previously in 35 % prestressed samples (35P1R28D40L), the pull-out energy still showed a decrease, likely influenced by the reduced peak load and the method of calculating the area from the peak load point. Similarly, in the 7-day release samples, a slight increase of 6 % was observed in the samples prestressed at 13 %. However, the positive impact of extending the release time was more significant at a higher prestress level of 35 %, as the samples exhibited an increase of 23 % in the pull-out energy over the control samples. This consistent increase in the pull-out energy with higher prestress levels resulted from the increased frictional force mentioned previously as a result of positive influence of the Hoyer's effect.

### 3.5. Effect of testing age

The change of the bond performance in prestressed samples with age (28 and 90 days) is summarised in Fig. 9, demonstrating variations in initial stiffness, peak load, and debonding energy at the peak load. Upon

inspection of the pull-out response at different ages (28 days and 90 days) for the 1-day release time samples, it can be observed that the specimens' age influenced the bond behaviour of the samples. For the samples at 13 % prestress level, initial stiffness decreased by 17 % at 90 days of age, while the ultimate bond load, debonding, and pull-out energy remained almost constant. This resulted in a slight 6 % increase in the amount of the absorbed energy (debonding energy) the sample could take, while the pull-out energy decreased slightly by 6 %. Contrarywise, at 35 % prestress level, samples exhibited varying behaviour, partially recovering some of the damaged interfacial bond stated earlier. This led to a significant increase in the peak load by 30 %, 68 % in debonding energy and a 26 % increase in pull-out energy, with stiffness remaining relatively stable. This improvement may be attributed to the continued hydration of the matrix with age. Increasing stiffness often improves stability but can decrease the composite's energy absorption and deformability, reducing debonding energy and vice versa. It's worth noting that debonding energy values can increase proportionally with the peak load of the samples, indicating a trade-off between stiffness and debonding energy that varies with the bond strength.

In contrast, the variation in the bond behaviour was comparatively less significant in the 7-day released samples (see Fig. 10) than in the 1-day release samples. At 13 % prestress, the initial stiffness exhibited a slight decrease, only 6 % over time. The pull-out peak load also had a variant behaviour and increased after the first 28 days by 7 % at the age of 90 days, while the debonding energy remained at a constant value of 251 N.mm. Pull-out energy however increased significantly by 24 %. At 35 % prestress, the sample's initial stiffness increased significantly by 30 %, with a slight decrease in the pull-out peak load by 10 %. This resulted in a more significant decrease of 34 % in debonding energy toughness, while pull-out energy showed a relatively smaller decrease of only 8 %, similar to the pull-out peak load.

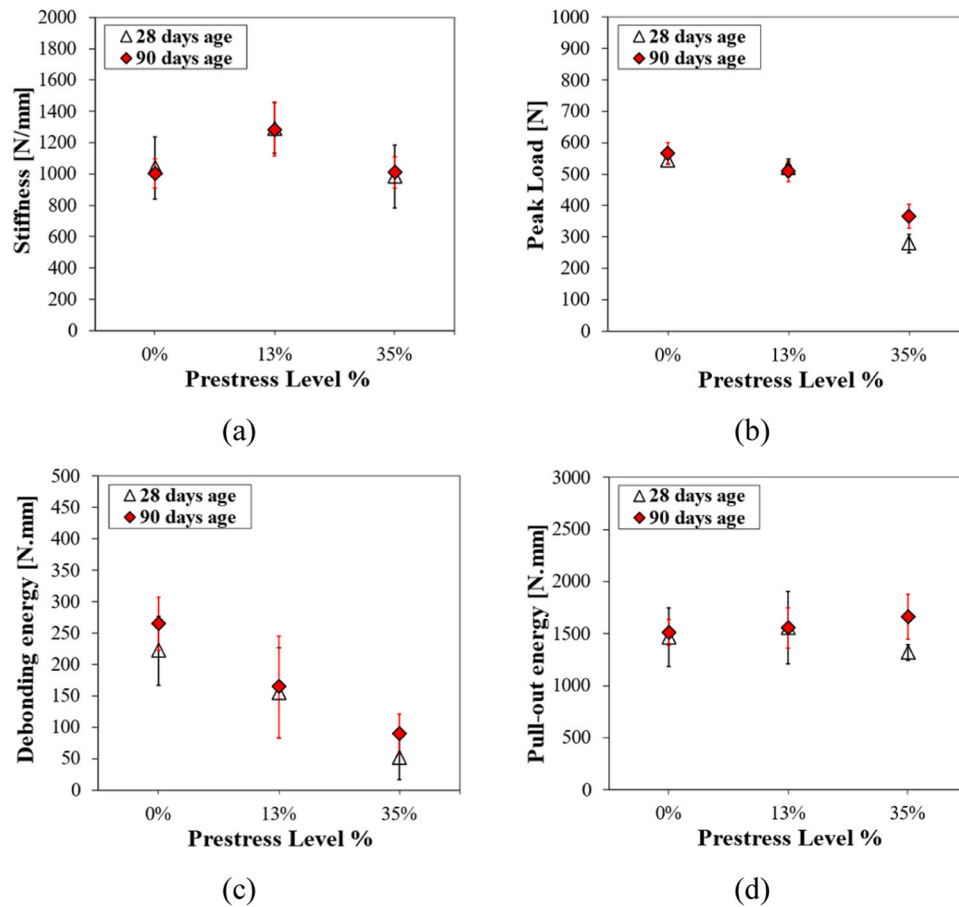


Fig. 9. Effect of testing age on 1-day release samples on: a) Initial Stiffness; b) Peak load; c) Debonding energy; and d) Pull-out energy for: 1-day release time samples.

### 3.6. Analytical estimation of the effect of prestressing on the crack spacing

The saturated crack spacing predictions for TRC composites can be effectively facilitated using the pull-out results obtained in this study [41]. Using the ACK-theory, the saturated crack spacing ( $X$ ) can be computed utilising the obtained average frictional stress ( $\tau_f$ ) and the tensile strength ( $\sigma_{mu}$ ) of the matrix, as represented by the following equation [52]:

$$X = 1.337 \frac{v_m \sigma_{mu} r}{v_f 2\tau_f}$$

Here,  $v_m$  denotes the volumetric fraction of the matrix, while  $v_f$  represents the volumetric fraction of the yarn, calculated as the area ratio between the yarn and the matrix cross-sectional area. The value of  $v_m$  can subsequently be determined as  $(1 - v_f)$ . Additionally,  $r$  signifies the yarn radius. It should be noted that a constant frictional stress at the debonded regions is assumed when using the ACK theory. The assumption of constant average frictional stress ( $\tau_f$ ) is based on the shear-lag model, which assumes continuity of displacements and tractions at the yarn interface, with constant shear stress ( $\tau$ ) along a debonded interface—a simplification proven effective in many experiments [23,52–56]. It is expected that the application of the ACK theory leads to a slight overestimation of the crack spacing in those samples. While application of more detailed analysis methods is suggested in future work, the provided calculations are not expected to change significantly as the slip-hardening slope coefficient was very small here (see Table 5). In the lack of direct tensile strength results,  $\sigma_{mu}$  can be inferred from the compressive or flexural tests conducted on the utilised matrix [57], see Table 6. Both approaches are followed here and the results are summarised in the table. It can be observed that the obtained

results are in close proximity with an average value of 5.07, which will be utilised in the crack spacing prediction model.

In this study two approaches were employed for the prediction of the crack spacing. The first approach utilised the calculated yarn area and radius based on the nominal thickness provided by the manufacturer’s datasheet, while the second approach incorporated the actual measured area of the yarns to account for the effect of prestressing. Consequently, variations in input parameters, such as the volumetric fractions of the yarn and the calculated frictional stress, are expected due to the differences in the yarn’s cross-sectional area. Table 7 presents the input parameters and the predicted values of the saturated crack spacing, based on the average calculated tensile strength. These predictions were made based on the assumption of double layers of textile reinforcement (mesh size = 25 mm) embedded in a 10 mm thick matrix, with a width of 90 mm.

Based on the results depicted in Fig. 11, it is anticipated that prestressing can effectively reduce the spacing of cracks with the increase in the prestress level. Specifically, at a 13 % prestress level, the crack spacing is predicted to undergo a significant decrease of 28 % and 27 % for the 1-day and 7-day release times, respectively. This indicates the effectiveness of prestressing in reducing crack spacing irrespective of release time at low prestress levels. However, at higher prestress levels, particularly at 35 %, the observed decrease in the bond strength in the samples released at 1-day led to a comparatively less significant reduction in crack spacing. This reduction is estimated at approximately 9 %. Conversely, for 7-day release samples, an increase in prestress level is expected to result in denser cracks, with a further anticipated decrease of 30 % at 35 % prestress level. Moreover, the calculated crack spacing utilising the nominal diameter provided by the manufacturer’s data sheet exhibits a slightly different trend, yielding values with a

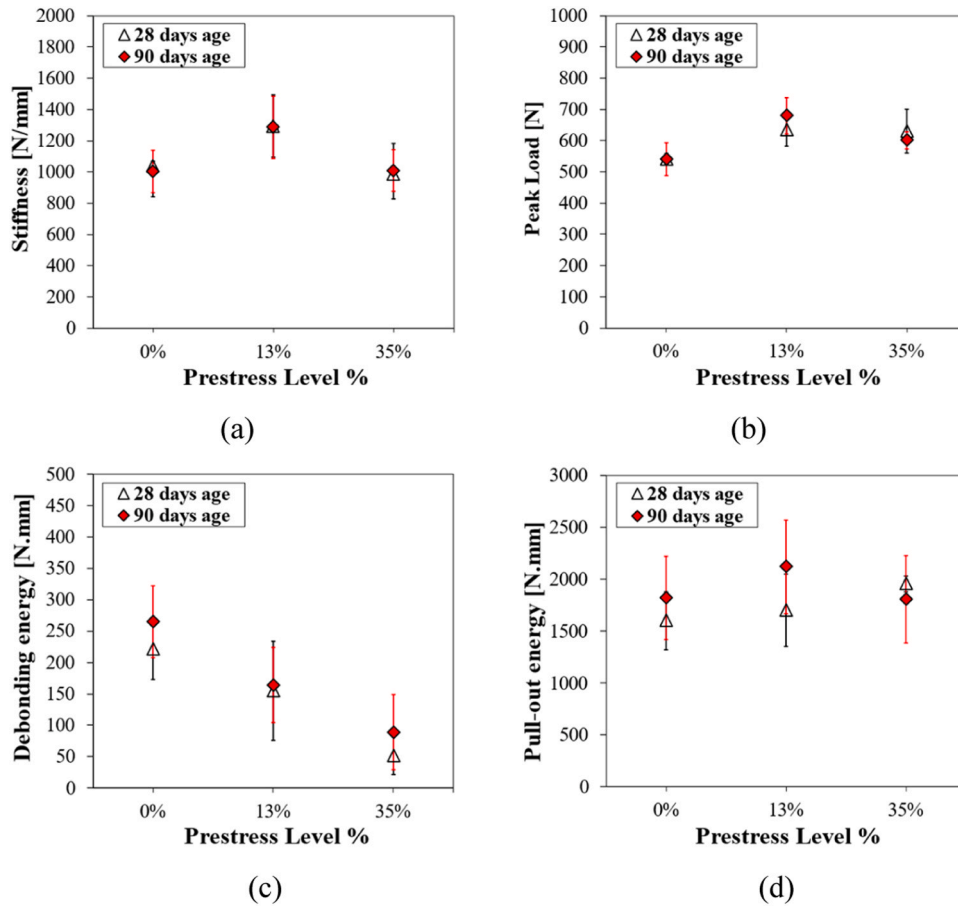


Fig. 10. Effect of testing age on 7-day release samples on: a) initial Stiffness; b) Peak load; c) Debonding energy; and d) Pull-out energy.

Table 6  
Tensile strength calculation.

Input parameter	Equation	$\sigma_{mu}$ [MPa]
Compressive strength ( $f_{cm}$ )	$2.12 \cdot \ln(1 + 0.1(f_{cm})) = 2.12 \ln(1 + 0.1(104))$	5.15
Flexural strength ( $f_{cm,fl}$ )	$\frac{0.06 \cdot h_b^{0.7}}{1 + 0.06 h_b^{0.7} f_{cm,fl}} = \frac{0.06 \cdot 40^{0.7}}{1 + 0.06 \cdot 40^{0.7}} \cdot 11.25$	4.98
Average		5.07

marginally higher range, accompanied by an approximate error of 15–17 %.

#### 4. Conclusions

This study focused on investigating the bond behaviour of non-prestressed and prestressed basalt Textile Reinforced Concrete. The investigation revolved around assessing the bond performance in terms

Table 7  
Crack spacing prediction.

ID	Tensile strength	calculation based on the measured area				calculation based on calculated area				$X_m/X_c$
		$v_f$	$v_m$	$\tau_f$	$X_m$	$v_f$	$v_m$	$\tau_f$	$X_c$	
0P0R28DB1	5.07	0.012	0.988	1.31	140.85	0.0082	0.9918	1.57	170.35	0.83
13P1R28D	5.07	0.011	0.989	1.88	102.02	0.0082	0.9918	2.22	120.87	0.84
35P1R28D	5.07	0.011	0.989	1.52	128.39	0.0082	0.9918	1.78	150.50	0.85
0P0R28DB7	5.07	0.012	0.988	1.45	129.52	0.0082	0.9918	1.73	155.10	0.84
13P7R28D	5.07	0.011	0.989	2.02	94.55	0.0082	0.9918	2.39	112.06	0.84
35P7R28D	5.07	0.011	0.989	2.14	91.03	0.0082	0.9918	2.51	106.91	0.85

of initial stiffness, pull-out load, and debonding energy while considering variables such as embedded length, prestressing level, prestress release time and the testing age. The findings yield the following conclusions:

- The predominant failure mode of non-prestressed samples across all considered embedded lengths (30–50 mm) was slippage, indicating a consistent behaviour in the bond failure mechanism. The observed increase in the average pull-out peak load of non-prestressed basalt textile with an extended embedded length suggests that the effective embedded length in this system exceeds the specified range.
- Prestressing significantly influenced bond behaviour, which was found to be dependent on both applied load and prestress release time, but not the failure mode. Independently from the prestress release times (1-day or 7-day), samples prestressed at lower load levels showed a higher bond's initial stiffness.
- Across all considered prestress levels, variations in peak load and bond stress were observed based on the prestress release time. Lower prestress levels (i.e., 13 %) generally enhanced the peak load and



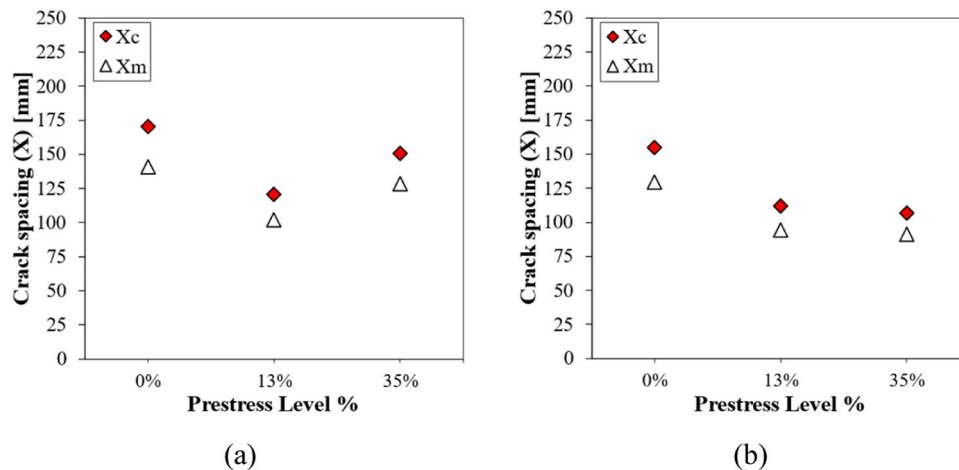


Fig. 11. Predicted crack spacing for a)1-day release time and b)7-day release time.

average bond strength, while releasing higher prestress levels at an early age of 1-day showed a degrading effect. However, extended prestress release times were crucial for achieving higher peak loads and average bond strength, with notable increases observed in samples subjected to a 7-day release time, particularly at a high prestress level of 35%. Therefore, caution is advised for releasing higher prestress levels within short periods, unless suitable hydration degree is achieved, necessitating additional measures for sufficient bond strength.

- The energy required for debonding exhibited similar trends to peak load and stiffness, with lower prestress levels generally resulting in higher debonding energy. However, releasing higher prestress levels at an early age showed a decreasing effect on debonding energy. Extended prestress release times were essential for achieving higher debonding energy, particularly at high prestress levels.
- Prestressing improved frictional stress and pull-out energy regardless of the release time, except for the case of 35% prestressed samples released at 1-day, where it remained constant. Debonding energy values were reduced with increasing prestress levels in 1-day release samples but exhibited enhancement in 7-day release samples at low and high prestress levels, highlighting the positive impact of prolonged release times on energy absorption.
- The average bond strength development remained insignificantly affected by mortar age beyond the initial 28 days for both prestressed and non-prestressed samples. An exception was noted for the 1-day release at 35% prestress level samples, where average bond strength demonstrated recovery over time, indicating resilience to initial bond damage.
- The obtained pull-out results can be used effectively with the ACK model to provide valuable insights into the effect of prestressing on the predicted crack spacing. The results showed a clear effect of prestressing on reducing the saturated crack spacing. It was also observed that the application of yarn's cross sectional obtained from the technical datasheets can lead to a 15–17% increased saturated crack spacing predictions.
- This study aimed to provide insights on the role of prestressing on the pullout response, further studies are still needed to better understand the complex stress state during pullout, particularly in prestressed samples. This includes investigating the role of embedded length and yarn geometry on the overall bond response.

#### CRediT authorship contribution statement

**Mohammed Hutaibat:** Writing – review & editing, Writing – original draft, Visualization, Validation, Methodology, Investigation, Formal analysis, Data curation, Conceptualization. **Bahman Ghiassi:** Writing –

review & editing, Writing – original draft, Supervision, Resources, Project administration, Methodology, Funding acquisition, Conceptualization. **Walid Tizani:** Writing – review & editing, Writing – original draft, Supervision, Investigation, Conceptualization.

#### Declaration of Competing Interest

The authors declare that they have no known competing financial interests or personal relationships that could have appeared to influence the work reported in this paper.

#### Data Availability

Data will be made available on request.

#### Acknowledgements

This work was partly supported by the Institute of Structural Engineers (ISTRUCTE) for the financial support received through research award 2068060-ISTRUCTE and Royal Society through research grant RG\R2\232149. The first author acknowledges the financial support provided by Middle East University (MEU) - Jordan.

#### References

- [1] M.K. Sambath, Sustainable performance criteria for prefabrication construction system, *Int. J. Sci. Res. Publ. (IJSRP)* 10 (2020) 455, <https://doi.org/10.29322/IJSRP.10.04.2020.p10052>.
- [2] J. Hegger, N. Will, H.N. Schneider, P. Kölzer, *Neue Bauteile aus textildbewehrtem Beton, Beton- und Stahlbetonbau* 99 (6) (2004) 482–487, <https://doi.org/10.1002/best.200490121>.
- [3] C.D. Johnston, *Fiber-Reinforced Cements and Concretes*, Crc Press, 2014, <https://doi.org/10.1201/9781482298154>.
- [4] R. Figueiro, C. Gonigho-Pereira, *Fibrous and a Composite Materials for Civil Engineering Applications*, Woodhead Publishing, 2011, pp. 216–249.
- [5] V. Dhand, G. Mittal, K.Y. Rhee, S.-J. Park, D. Hui, A short review on basalt fiber reinforced polymer composites, *Compos. Part B: Eng.* 73 (2015) 166–180, <https://doi.org/10.1016/j.compositesb.2014.12.011>.
- [6] J. Sim, C. Park, D.Y. Moon, Characteristics of basalt fiber as a strengthening material for concrete structures, *Compos. Part B: Eng.* 36 (6) (2005) 504–512, <https://doi.org/10.1016/j.compositesb.2005.02.002>.
- [7] M. Hutaibat, B. Ghiassi, W. Tizani, Flexural behaviour of concrete thin sheets prestressed with basalt-textile reinforcement, *Constr. Build. Mater.* 404 (2023) 133213, <https://doi.org/10.1016/j.conbuildmat.2023.133213>.
- [8] S. Gopinath, R. Gettu, N.R. Iyer, Influence of prestressing the textile on the tensile behaviour of textile reinforced concrete, *Mater. Struct.* 51 (3) (2018) 64, <https://doi.org/10.1617/s11527-018-1194-z>.
- [9] A. Peled, Pre-tensioning of fabrics in cement-based composites, *Cem. Concr. Res.* 37 (2007) 805–813, <https://doi.org/10.1016/j.cemconres.2007.02.010>.
- [10] B. Zastrau, M. Richter, I. Lepenies, On the Analytical Solution of Pullout Phenomena in Textile Reinforced Concrete, *J. Eng. Mater. Technol.* 125 (1) (2002) 38–43, <https://doi.org/10.1115/1.1526125>.

- [11] C. Soranakom, B. Mobasher, Geometrical and mechanical aspects of fabric bonding and pullout in cement composites, *Mater. Struct.* 42 (6) (2009) 765–777, <https://doi.org/10.1617/s11527-008-9422-6>.
- [12] J. Deluce, F. Vecchio, Cracking behavior of steel fiber-reinforced concrete members containing conventional reinforcement, *Acids Struct. J.* 110 (2013) 481–490.
- [13] A.E. Naaman, 18 - Thin TRC products: Status, outlook, and future directions, in: T. Triantafillou (Ed.), *Textile Fibre Composites in Civil Engineering*, Woodhead Publishing, 2016, pp. 413–439.
- [14] U. Häußler-Combe, J. Hartig, Bond and failure mechanisms of textile reinforced concrete (TRC) under uniaxial tensile loading, *Cem. Concr. Compos.* 29 (4) (2007) 279–289, <https://doi.org/10.1016/j.cemconcomp.2006.12.012>.
- [15] N. Williams Portal, L. Nyholm Thrane, K. Lundgren, Flexural behaviour of textile reinforced concrete composites: experimental and numerical evaluation, *Mater. Struct.* 50 (1) (2016) 4, <https://doi.org/10.1617/s11527-016-0882-9>.
- [16] M. Krüger, Vorgespannter Textilbewehrter, Beton (Pre stressed textile reinforced concrete), Philosophy doctoral thesis, Stuttgart, Universität Stuttgart, Fakultät Bau- und Umweltingenieurwissenschaften, Diss (2004), <https://doi.org/10.18419/opus-192>.
- [17] J. Hegger, O. Bruckermann, R. Chudoba, 134. A smeared bond-slip relation for multi-filament yarns embedded in fine concrete. 6th International RILEM Symposium on Fibre Reinforced Concretes, RILEM Publications SARL, 2004, pp. 1453–1462.
- [18] B. Banholzer, T. Brockmann, W. Brameshuber, Material and bonding characteristics for dimensioning and modelling of textile reinforced concrete (TRC) elements, *Mater. Struct.* 39 (8) (2006) 749–763, <https://doi.org/10.1617/s11527-006-9140-x>.
- [19] M. Glowania, T. Gries, J. Schoene, M. Schleser, U. Reisgen, Innovative coating technology for textile reinforcements of concrete applications, *Key Eng. Mater.* 466 (2011) 167–173, <https://doi.org/10.4028/www.scientific.net/KEM.466.167>.
- [20] A. Bentur, A. Peled, D. Yankelevsky, Enhanced bonding of low modulus polymer fibers-cement matrix by means of crimped geometry, *Cem. Concr. Res.* 27 (7) (1997) 1099–1111, [https://doi.org/10.1016/S0008-8846\(97\)00088-4](https://doi.org/10.1016/S0008-8846(97)00088-4).
- [21] A. Peled, B. Mobasher, Pultruded fabric-cement composites, *Acids Mater. J.* 102 (2005) 15–23.
- [22] A. Peled, B. Mobasher, S. Sueki, Technology methods in textile cement-based composites, *concrete science and engineering*, RILEM Proc. PRO (2004) 187–202.
- [23] S. Sueki, C. Soranakom, B. Mobasher, A. Peled, Pullout-slip response of fabrics embedded in a cement paste matrix, *J. Mater. Civ. Eng.* 19 (9) (2007) 718–727, [https://doi.org/10.1061/\(ASCE\)0899-1561\(2007\)19:9\(718\)](https://doi.org/10.1061/(ASCE)0899-1561(2007)19:9(718)).
- [24] M. Krüger, H.W. Reinhardt, M. Fichtlscherer, Bond Behaviour of Textile Reinforcement in Reinforced and Prestressed, 2001.
- [25] S. Xu, M. Krüger, H.W. Reinhardt, J. Özbolt, Bond characteristics of carbon, alkali resistant glass, and aramid textiles in mortar, *J. Mater. Civ. Eng.* 16 (4) (2004) 356–364, [https://doi.org/10.1061/\(ASCE\)0899-1561\(2004\)16:4\(356\)](https://doi.org/10.1061/(ASCE)0899-1561(2004)16:4(356)).
- [26] S. Xu, H. Li, Bond properties and experimental methods of textile reinforced concrete, *J. Wuhan. Univ. Technol. -Mater. Sci. Ed.* 22 (3) (2007) 529–532, <https://doi.org/10.1007/s11595-006-3529-9>.
- [27] ASTM C109 / C109M-16a, Standard Test Method for Compressive Strength of Hydraulic Cement Mortars (Using 2-in. or [50-mm] Cube Specimens), ASTM International, West Conshohocken, PA, 2016., ([www.astm.org](http://www.astm.org)).
- [28] British Standards Institution (2019) BS EN 12390-3:2019: Testing hardened concrete: Compressive strength of test specimens, British Standards Institution, London, 2019.
- [29] British Standards Institution (2019) BS EN 1015-11:2019: Methods of test for mortar for masonry: Determination of flexural and compressive strength of hardened mortar, British Standards Institution, London, 2019.
- [30] A. Dalalbashi, B. Ghiassi, D.V. Oliveira, A. Freitas, Effect of test setup on the fiber-to-mortar pull-out response in TRM composites: experimental and analytical modeling, *Compos. Part B: Eng.* 143 (2018) 250–268, <https://doi.org/10.1016/j.compositesb.2018.02.010>.
- [31] B. Ghiassi, D.V. Oliveira, V. Marques, E. Soares, H. Maljaee, Multi-level characterization of steel reinforced mortars for strengthening of masonry structures, *Mater. Des.* 110 (2016) 903–913, <https://doi.org/10.1016/j.matdes.2016.08.034>.
- [32] A. Dalalbashi, S. De Santis, B. Ghiassi, D. Oliveira, Slip rate effects and cyclic behaviour of textile-to-matrix bond in textile reinforced mortar composites, *Mater. Struct.* 54 (2021), <https://doi.org/10.1617/s11527-021-01706-w>.
- [33] A. Dalalbashi, B. Ghiassi, D.V. Oliveira, Textile-to-mortar bond behavior: an analytical study, *Constr. Build. Mater.* 282 (2021) 122639, <https://doi.org/10.1016/j.conbuildmat.2021.122639>.
- [34] N. Williams Portal, I. Fernandez Perez, L. Nyholm Thrane, K. Lundgren, Pull-out of textile reinforcement in concrete, *Constr. Build. Mater.* 71 (2014) 63–71, <https://doi.org/10.1016/j.conbuildmat.2014.08.014>.
- [35] Building code requirements for structural concrete (ACI 318-95) and commentary (ACI 318R-95), American Concrete Institute, Farmington Hills, MI, 1995.
- [36] A.A.o.S. Highway, T. Officials, AASHTO LRFD Bridge Design Specifications - 1996 Interim: (Metric Units), American Association of State Highway & Transportation Officials 1996.
- [37] R. El-Hacha, Prestressing Concrete Structures with FRP Tendons (ACI 440.4R-04), 2005, [https://doi.org/10.1061/40753\(171\)160](https://doi.org/10.1061/40753(171)160).
- [38] J. Shi, X. Wang, H. Huang, Z. Wu, Relaxation behavior of prestressing basalt fiber-reinforced polymer tendons considering anchorage slippage, *J. Compos. Mater.* 51 (9) (2016) 1275–1284, <https://doi.org/10.1177/0021998316673893>.
- [39] M.J. Shannag, R. Brincker, W. Hansen, Pullout behavior of steel fibers from cement-based composites, *Cem. Concr. Res.* 27 (6) (1997) 925–936, [https://doi.org/10.1016/S0008-8846\(97\)00061-6](https://doi.org/10.1016/S0008-8846(97)00061-6).
- [40] E. Lorenz, R. Ortlepp, Bond behavior of textile reinforcements - development of a pull-out test and modeling of the respective bond versus slip relation, in: G. J. Parra-Montesinos, H.W. Reinhardt, A.E. Naaman (Eds.), *High Performance Fiber Reinforced Cement Composites 6: HPRCC 6*, Springer, Netherlands, Dordrecht, 2012, pp. 479–486.
- [41] A. Dalalbashi, B. Ghiassi, D.V. Oliveira, A multi-level investigation on the mechanical response of TRM-strengthened masonry, *Mater. Struct.* 54 (6) (2021) 224, <https://doi.org/10.1617/s11527-021-01817-4>.
- [42] J.M. Alwan, A.E. Naaman, W. Hansen, Pull-out work of steel fibers from cementitious composites: analytical investigation, *Cem. Concr. Compos.* 13 (4) (1991) 247–255, [https://doi.org/10.1016/0958-9465\(91\)90030-L](https://doi.org/10.1016/0958-9465(91)90030-L).
- [43] ACI Committee, Building code requirements for structural concrete (ACI 318-08) and commentary, American Concrete Institute, 2008.
- [44] J. Hegger, D. Tuchlinski, B. Kommer, Bond anchorage behavior and shear capacity of ultra high performance concrete beams, 2004.
- [45] N.G. Domenico, Z.I. Mahmoud, S.H. Rizdalla, Bond properties of carbon fiber composite prestressing strands, *Struct. J.* 95 (3) (1998) 281–290, <https://doi.org/10.14359/546>.
- [46] M. Zawam, K.A. Soudki, Factors affecting the transfer length of prestressed GFRP bars in concrete, 16, *Spec. Publ.* 322 (21) (2018) 1–21, <https://doi.org/10.14359/51706972>.
- [47] Z. Lin, T. Kanda, V.C. Li, On interface property characterization and performance of fiber reinforced cementitious, *Composites* (1999).
- [48] E.A. Schaufert, G. Cusatis, D. Pelessone, J. O'Daniel, J.T. Baylot, Lattice discrete particle model for fiber-reinforced concrete. II: tensile fracture and multiaxial loading behavior, *J. Eng. Mech. -asce* 138 (2012) 834–841, [https://doi.org/10.1061/\(ASCE\)EM.1943-7889.0000392](https://doi.org/10.1061/(ASCE)EM.1943-7889.0000392).
- [49] G. Nilakantan, R.L. Merrill, M. Keefe, J.W. Gillespie, E.D. Wetzel, Experimental investigation of the role of frictional yarn pull-out and windowing on the probabilistic impact response of kevlar fabrics, *Compos. Part B: Eng.* 68 (2015) 215–229, <https://doi.org/10.1016/j.compositesb.2014.08.033>.
- [50] Z. Lin, V.C. Li, Crack bridging in fiber reinforced cementitious composites with slip-hardening interfaces, *J. Mech. Phys. Solids* 45 (5) (1997) 763–787, [https://doi.org/10.1016/S0022-5096\(96\)00095-6](https://doi.org/10.1016/S0022-5096(96)00095-6).
- [51] C. Redon, V.C. Li, C. Wu, H. Hoshino, T. Saito, A. Ogawa, Measuring and modifying interface properties of PVA fibers in ECC matrix, *J. Mater. Civ. Eng.* 13 (2001) 399–406, [https://doi.org/10.1061/\(ASCE\)0899-1561\(2001\)13:6\(399\)](https://doi.org/10.1061/(ASCE)0899-1561(2001)13:6(399)).
- [52] H. Cuyppers, J. Wastiels, Stochastic matrix-cracking model for textile reinforced cementitious composites under tensile loading, *Mater. Struct.* 39 (8) (2006) 777–786, <https://doi.org/10.1617/s11527-005-9053-0>.
- [53] C.-H. Hsueh, Interfacial debonding and fiber pull-out stresses of fiber-reinforced composites, *Mater. Sci. Eng.: A* 123 (1) (1990) 1–11, [https://doi.org/10.1016/0921-5093\(90\)90203-F](https://doi.org/10.1016/0921-5093(90)90203-F).
- [54] D.B. Marshall, Analysis of fiber debonding and sliding experiments in brittle matrix composites, *Acta Metall. Et. Mater.* 40 (3) (1992) 427–441, [https://doi.org/10.1016/0956-7151\(92\)90391-Q](https://doi.org/10.1016/0956-7151(92)90391-Q).
- [55] D.B. Marshall, W.C. Oliver, Measurement of interfacial mechanical properties in fiber-reinforced ceramic composites, *J. Am. Ceram. Soc.* 70 (8) (1987) 542–548, <https://doi.org/10.1111/j.1151-2916.1987.tb05702.x>.
- [56] B. Mobasher, *Mechanics of Fiber and Textile Reinforced Cement Composites*, CRC press, 2011, <https://doi.org/10.1201/b11181>.
- [57] b.t. Fédération internationale du, Fib model code for concrete structures 2010, Ernst & Sohn, a Wiley brand, Lausanne, Switzerland, 2013, <https://www.doi.org/10.1002/9783433604090>.